POLITECNICO DI TORINO
Repository ISTITUZIONALE

A passive two-way microfluidic device for low volume blood-plasma separation

(Article begins on next page)

13 March 2024

Accepted Manuscript

A passive two-way microfluidic device for low volume blood-plasma separation

L. Spigarelli, V. Bertana, D. Marchisio, L. Scaltrito, S. Ferrero, M. Cocuzza, S.L. Marasso, G. Canavese, C.F. Pirri

Please cite this article as: L. Spigarelli, V. Bertana, D. Marchisio, et al., A passive two-way microfluidic device for low volume blood-plasma separation, Microelectronic Engineering, https://doi.org/10.1016/j.mee.2019.02.011

A passive two-way microfluidic device for low volume blood-plasma separation

L Spigarelli[a], V Bertana[b,*] valentina.bertana@polito.it, D Marchisio[a], L Scaltrito[b], S Ferrero[b], M Cocuzza[b,c], S L Marasso[b,c], G Canavese[a], C F Pirri[b]

[a]Department of Applied Science and Technology, Politecnico di Torino, Corso Duca degli Abruzzi 24, 10129 Torino, Italy
[b]Chilab - Materials and Microsystems Laboratory - DISAT Politecnico di Torino, Via Lungo Piazza d'Armi 6, 10034 Chivasso (Turin), Italy
[c]CNR-IMEM, Parco Area delle Scienze, 37a, 43124 Parma, Italy

[*]Corresponding author.

Abstract

Blood-plasma separation is one of the main concerns for Point-of-Care devices seeking to retain cells of interest or analyze plasma biomarkers. The present work describes a novel passive device based on size-exclusion method. Starting from a particulate-trap-like filter, numerical simulations in ANSYS Fluent were performed in order to optimize the geometry for blood-plasma separation. The final layout was then embedded inside a microfluidic channel and the related master produced with standard cleanroom processes. A 1 mm thick Cyclic Olefin Copolymer wafer was chosen for hot embossing replication, since Cyclic Olefin Copolymer is a transparent, solvent-resistant and medical-grade material. Moreover, the adopted process is easily scalable to industrial levels. The filtering efficiency was finally assessed with a 4 µm fluorescent beads dispersion, mimicking the erythrocytes average diameter of 8 µm. No fluorescent particles were observed downstream of the filter after filtration, thus all the beads were retained by the optimized filtering structure.

1. Introduction

Nowadays, one of the main concerns for health operators is to accomplish early diagnosis, particularly in case of genetic hereditary diseases and tumors [1], [2]. The simplest way to gain the patient clinical picture is surely a liquid biopsy, i.e. blood analysis, which is quite easily available and may carry different biomarkers and health levels [3]. Standard approach for blood tests requires expensive and cumbersome instruments for sample preparation before analysis [4]. Moreover, large volumes of blood of the order of milliliters are required [5]. With a focus on Point-of-Care diagnostics (POC), especially where laboratory facilities are absent or difficult to reach [6], many different microfluidic platforms have been developed for blood fractionation and sample preparation. Sample preparation indeed is a key-part for a liquid biopsy to be performed involving purification [7], [8], enrichment or labeling [5]. In detail, most of the preparation techniques performed in Lab-on-a-Chips are devoted to cells trapping [9], [10] or cells exclusion and plasma analysis [11]–[15] (e.g. for the detection of disease biomarkers [16], [17]). The common denominator between them is the ease of use: low blood volume, rapid response and only little training are required [5]. In this work, a microfluidic device for blood plasma separation embedding a filter based on size-exclusion was designed, aiming to overcome the common drawbacks encountered in previous works. Size exclusion was chosen since it is a passive technique [18] which has shown promising results in terms of separation efficiency and also allows for other processes integration in a single chip [19]. The filtrating structure is embedded in the microfluidic device and produced with the same material at the same time, thus avoiding unwanted leakage issues from commercial filter integration with an existing channel [20]–[23]. Moreover, the whole device was studied to allow the de-clogging by the application of a reversal flow (from outlet to inlet), similarly to the capture/release microchip proposed by Li et al. [24], and without the need for device opening and re-sealing [19]. The whole filter development was based on and supported by fluid-dynamic simulations (CFD) carried out with the commercial solver ANSYS Fluent 18.0®. Considering as a reference a standard filter configuration composed by posts oriented perpendicularly to the flow direction, different geometries have been studied aiming to enhance filtering efficiency and retard clogging. The computational demand and the complexity of the system were common problems for the optimization of the microfluidic device. This was solved dividing the filter in equal portions and considering each portion as an analogous electrical circuit, as illustrated by Yang et al. [25]. Due to the low aspect ratio of the cross-section, the resulted pressure drop was one of the main parameters to take into account. Since friction resistances are supposed to be the main cause of the pressure drops along the channel, Hagen-Poiseuille equation [26] was considered to validate numerical simulation. Similar devices were proposed by Andersson et al. [27] and Ji et al. [28]. Differently from these works, which certainly represent a milestone in microchip fabrication for blood separation, the present investigation, based on computational fluid dynamic, was focused on the optimization of the filter layout to increase separation performance and reduce process cost.

2. Numerical model

2.1 Simulation domain and parameters

The filter object of the study was intended to be set inside a microfluidic channel with dimensions 630 μm x 15 μm (WxH) to filter particles bigger than 2 μm (e.g. blood cells). The simplest structure would be a porous wall, orthogonal to the channel, composed by adjacent posts (as the ones in Figure 1) characterized by a total pore area of 540 μm^2. One of the objectives of the present work was to enhance the filtering area; for this reason, a filtering module analogous to a particulate wall flow filter module [29] was proposed (Figure 1).
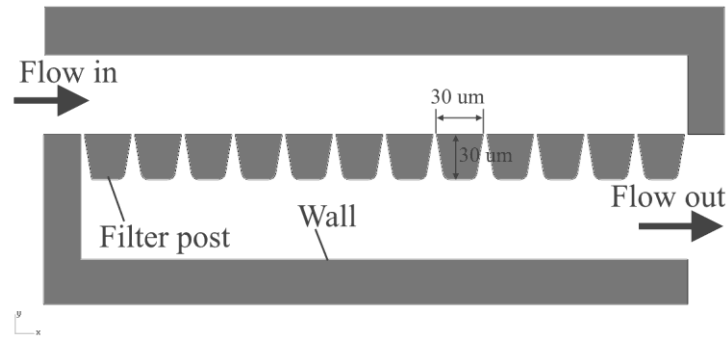
Figure 1 Geometrical characteristics of the filtering module. The distance between walls and posts is 52.5 μm, both upstream and downstream the posts, and the minimum distance between the posts is 2 μm.

The filter posts have a trapezoidal shape with the major base and the height equal to 30 μm. The walls limiting each module are 20 μm large. Such dimensions were imposed with a view to the subsequent fabrication for experimental validation, therefore discussed later (See Experimental section).

The module layout reported in Figure 1 represented the starting point for the filter optimization, which involved both the tilting of walls and posts and, consequently, the setting of the correct number of modules to fit the microfluidic channel width.

2.2 Governing equations

First, the continuity equation must be considered, whose general formula is expressed in equation 1.

$$\partial_t \rho = - \nabla \cdot (\rho \boldsymbol{v}) \qquad (1)$$

Here ρ is the fluid density and $\boldsymbol{v}$ is the velocity vector. When the fluid sample is liquid, as usually happens in microfluidics, this could be assumed as incompressible. This assumption means that density does not change in space and time, and equation (1) is simplified to equation 2,

$$\nabla \cdot \boldsymbol{v} = 0 \qquad (2)$$

The second governing equation is the so called Navier-Stokes equation. This equation establishes a relationship between the velocity field and the momentum conservation and the momentum density, whose Eulerian form for an incompressible fluid is expressed in equation 3.

$$\rho[\partial_t \boldsymbol{v} + (\boldsymbol{v} \cdot \nabla)\boldsymbol{v}] = - \nabla p + \mu \nabla^2 \boldsymbol{v} + \rho g \qquad (3)$$

In the above formula, p is the pressure and g is the gravitational acceleration, whose corresponding body force is usually neglected at the microfluidic scale. When Newtonian fluids are treated, coefficient μ, the dynamic viscosity, can be considered constant at fixed temperature. One of the main non-dimensional number used in microfluidics is the Reynolds number, expressed in equation 4, where v is the mean velocity of the fluid and L is the characteristic size of the system [30].

$$Re = \frac{\rho v L}{\mu} \qquad (4)$$

This number is important because in a microfluidic channel is low, thus inertial effects can be neglected [31].

2.3 Boundary conditions

Since the filtration phenomena are focused mainly on the transversal and longitudinal length, a 3D planarly symmetric geometry was used for the numerical studies presented in this paper. In the experimental setup the fluid was pushed through the channel using a syringe pump and this was simulated imposing a constant velocity of 3.42×10^{-3} m/s at the inlet boundary condition, corresponding to a flow rate of 20 μl/min. Atmospheric pressure was set at the outlet. To simplify the model the roughness of the walls was neglected, and the no-slip condition was chosen at the boundaries. The geometry was filled with water at 25° C, whose properties are listed in Table 1.

Table 1 Properties of water at 25°C

Property	Symbol	Value

| Fluid Density | ρ | $998.2 \left[\frac{kg}{m^3}\right]$ |
| Dynamic viscosity | μ | $1.003 \times 10^{-3} \left[\frac{kg}{m \cdot s}\right]$ |

2.4 Convergence Analysis

An unstructured tetrahedral mesh was used in this study. The meshing tool inside the ANSYS package was used for generating and analysing mesh statistics and quality. Initially a maximum element size in the bulk of the channel was chosen as 5 µm and then it was decreased to perform the convergence analysis. For the walls a program-controlled inflation was used. The number of steps to reach a residual in continuity, x-velocity, y-velocity and z-velocity of 1×10^{-5}, was recorded. The element size that guarantees a convergence in a good computational time was 2 µm, so it was used in the following as default size (for further information see *Supplementary Material*). With this parameter the mesh was composed of about 1×10^7 elements and 4×10^6 nodes.

3. Experimental

The filter layout resulting from the numerical optimization was embedded inside a 1 cm long microfluidic channel to be fabricated and tested.

3.1 Design of the filtering structure

As reported in Section 2.1, the filtering structure is composed by a fixed number of modules, each comprising trapezoidal posts designed to be 2 µm apart each other, thus determining the cutoff size. The dimension of the components (posts and walls) were chosen as the best compromise in terms of fabrication accuracy with respect to the final device fabrication process involving lithography, dry etching and thermal embossing. Previous etching and de-molding tests revealed that an approximately cuboid hole of 30 µm x 30 µm could ensure a satisfying filling of the polymer during embossing and a good detachment of the replica from the master. Then, the trapezoidal shape was selected and oriented so that the tapered constriction was opposite to the forward flow. Therefore, during the filtration phase (forward flow) the particles bigger than the pores are efficiently blocked. In case some particles are able to pass through, they could squeeze through the constrictions [32] during the de-clogging phase (backward flow) and return to the "unfiltered side" to be hopefully trapped in a second moment.

3.2 Fabrication of the filtering device

The whole filtering device was produced in a three-steps process: master fabrication, hot embossing replication and bonding. The master fabrication was the most time-consuming and articulated step and it consisted of lithography and dry etching. A 2-inches silicon wafer finished with 1 µm silicon oxide was firstly coated by a thin layer of the positive resist AZ1518 (MicroChemicals GmbH). The adhesion of the resist on the wafer surface was ensured by a previous spin coating of an adhesion promoter (Ti Prime – MicroChemicals GmbH). Then, in order to accelerate the whole process, for the first prototypes the lithography consisted in the direct writing of six channel geometries (Figure 2a) on the wafer surface with the Laser Writer (LW405 - Microtech). The resist was developed in AZ400K developer, thus dissolving the resist in the irradiated area and making the silicon oxide removable via Buffered Oxide Etch (BOE, HF:NH$_4$F=1:7) wet etching. The wafer was then rinsed in acetone to remove the resist thus showing the six device geometries etched on its oxide layer; the wafer was then subjected to anisotropic dry Deep Reactive Ion Etching (ICP-DRIE Oxford Plasmalab 100) through a conventional cryogenic process [33]. The master appeared as in Figure 2b. Afterwards, the remaining 1 µm oxide layer, which served as a protective mask for dry etching, was removed by BOE wet etching and the wafer divided into six separate masters by laser cutting.
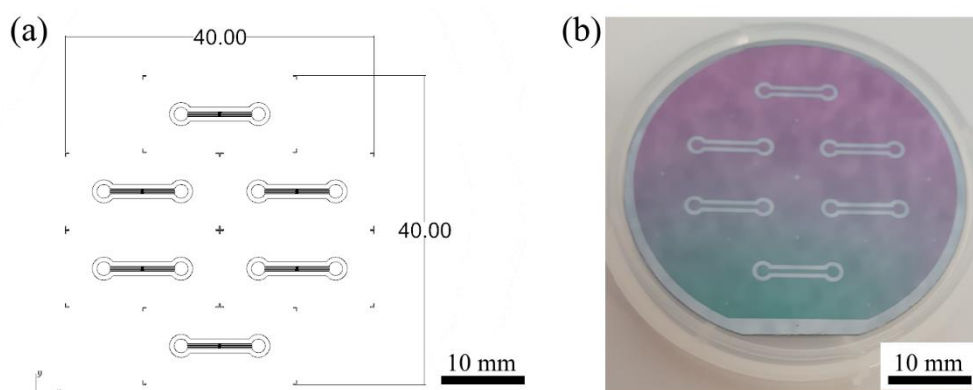
Figure 2 Fabrication of device master: (a) CAD geometry for a six-replica master; (b) Final silicon master before SiO$_2$ removal

For hot embossing replication, one of the masters was properly fixed to the upper plate of the hot embossing machine (HEX01 - JENOPTIK Mikrotechnik) and pressed onto a 1 mm thick Cyclic Olefin Copolymer (COC, Topas) foil for 240 s at 165 °C with a 2500 N load. The obtained replica was then thermally coupled to a 1 mm thick COC piece of foil with the same dimension and with two holes drilled in correspondence with the inlet/outlet geometry for 360 s at 115 °C with a 280 N load with the same equipment employed for hot embossing. Before coupling, the two COC parts were carefully rinsed in isopropanol (IPA) to remove possible dirt traces deriving from successive manipulations and aligned under a digital microscope (DVM2500 - LEICA). Profilometric characterization both of the master and the device are reported in the *Supplementary Material*. The final device appears as reported in Figure 3.
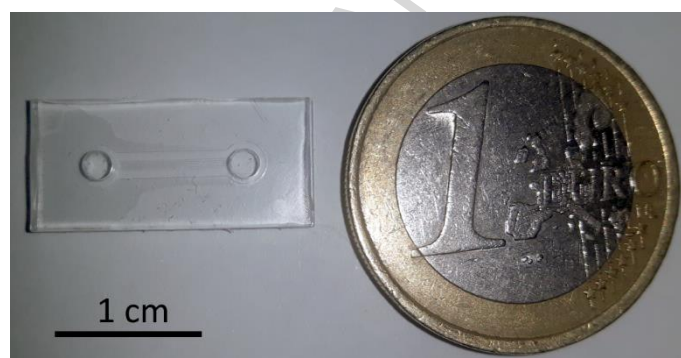

Figure 3 Filtration device after COC-COC bonding.

3.3 Fluorescence microscopy tests

The efficiency characterization of the proposed filter consisted in forcing fluorescent beads dispersion flowing through the filter, as reported in [34]. The fluorescent beads dispersion was prepared by adding 50 μl of green polystyrene fluorescent particle preparation (FluoSphere – ThermoFisher used as received at a concentration of c.a. $5x10^8$ particles/ml) to 1 ml of deionized water. The channel was previously filled with deionized water; the flow inside the device was performed by a syringe pump system comprising a 250 μl Hamilton Gastight syringe, a New Era NE1000 syringe pump and polyurethane tubing (SMC TU0212C-20). Tubing connect the outlet of the device with the syringe and are fixed at the device side by means of a PDMS adaptor (see *Supplementary Material*); the efficiency test started when 15 μl of fluorescent dispersion were pipetted inside the inlet of the channel and withdrawn at 5 μl/min for 3 minutes. The filter efficiency was evaluated by observing the fluorescent flow through the filter under the 20X objective of a fluorescent microscope Nikon Eclipse Ti mounting a green filter (acquisition at 9.8 ms frame rate).

3.4 Pressure tests

Pressure tests were conducted to both characterize the device and validate the data obtained from numerical analysis. The experimental setup was adapted from the one employed for fluorescence microscopy tests, with the only difference that tubing was connecting the syringe (containing deionized water) to the inlet through a

three-way valve. The third outlet of the valve served as connection point for the pressure sensor (Honeywell Microswitch - bridge pressure sensor 26PC Series) and data acquired as described in [35]. Pressure drop along the whole channel was acquired with an imposed 10 μl/min flow, which is typical for blood filtration [28]. Three data series were acquired, starting from the activation of syringe pump for deionized water infusion until reaching a pressure plateau (denoting an equilibrium state). For each series, the pressure value deriving from the mechanical connection between channel and tubing was treated as an offset and subtracted from the acquired values. Then, the maximum pressure value (corresponding to the plateau value) was extrapolated and, finally, the three pressure values from the three measurement series were averaged.

4. Results and discussion

4.1 Design optimization with CFD

One of the main purposes of the proposed numerical simulations was to investigate the fluid-dynamics of the system with the aim of optimizing the design of the device, focusing in detail in proximity of the filter. Qualitative and quantitative analyses for different geometries were performed in order to obtain a good compromise between mass flow rate and pressure drops in the whole device. As mentioned above, the filter module showed in Figure 1 was the starting point of the study and step by step the layout was changed. An overall framework of the optimization flow is shown in Figure 4.
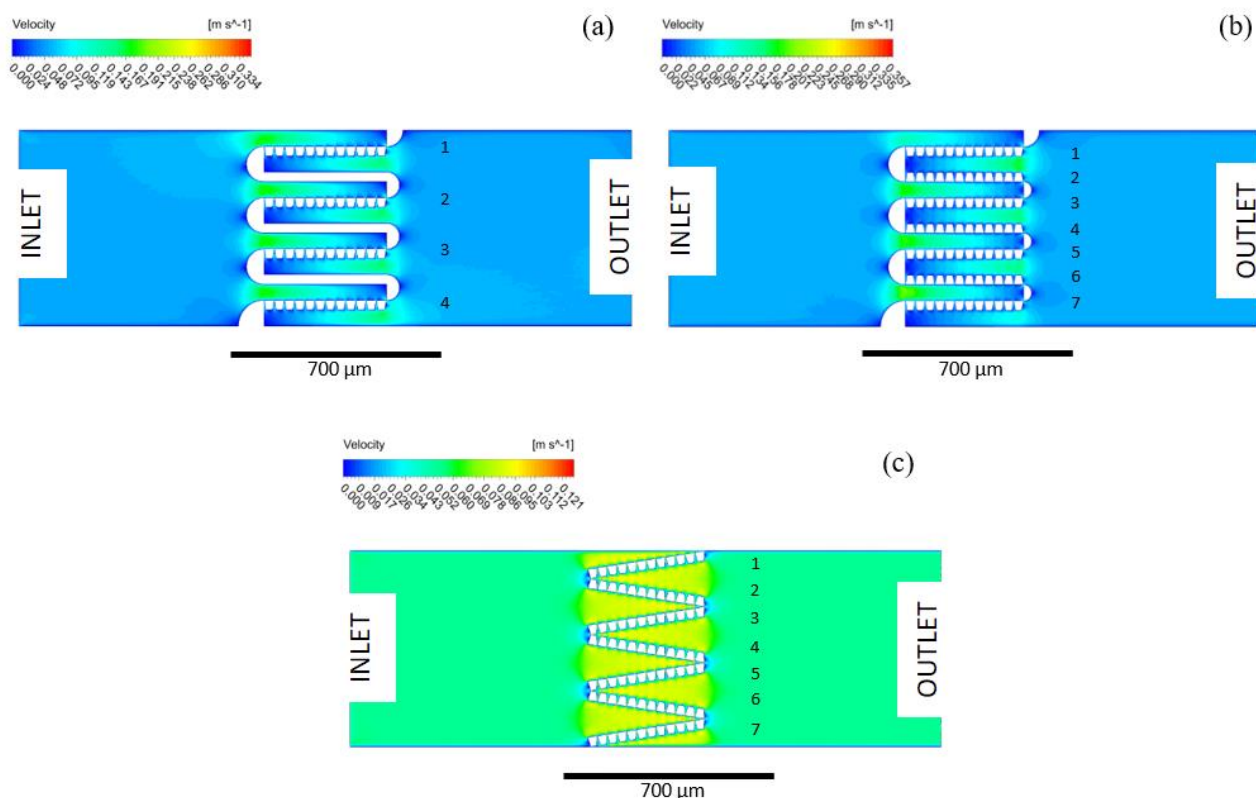

Figure 4 Velocity contour plots of the three investigated layouts

The first layout (Figure 4a) was designed by replicating four times the module reported in Figure 1 along the channel section. In this case, the total pore area is equal to 1560 μm^2. As can be seen, the velocity field seemed homogeneous through all the filter modules, but a deeper study of the mass flow rate underlined an uneven mass flow rate through the whole filter. In particular a peak, as illustrated in Figure 5, was observed in the last module (labelled with number 4). An attempt to reduce the mass flow heterogeneity along the modules and at the same time enhance the filtering area was made. The filtering modules were increased from four to seven (layout in Figure 4b) by replacing the walls with posts arrays. Now the total pore area is increased to 2730 μm^2, but unfortunately the mass flow rate was again found to be uneven, as the values reported in Figure 5 demonstrate. This can be explained with the asymmetry of the filter from the centre of

the channel. Trying to overcome the raised issues, the filter layout reported in Figure 4c was proposed: the filtering modules were set constant and tilted until covering the whole channel section (tilting angle 8.4°) without the aid of compact and closed structures (the semi-circular ones in Figure 4a and Figure 4b). The enhanced symmetry and the tilted angle helped to homogenize mass flow rate, keeping it almost constant among the modules (Figure 5) and equal to 5.2 x 10^{-8} kg/s. Moreover, the unwanted stagnant regions [28] were significantly reduced (zero velocity areas in the contour plots of Figure 4), as well as the maximum flow velocity through the filter which could mean lower shear stresses on the blood particles.
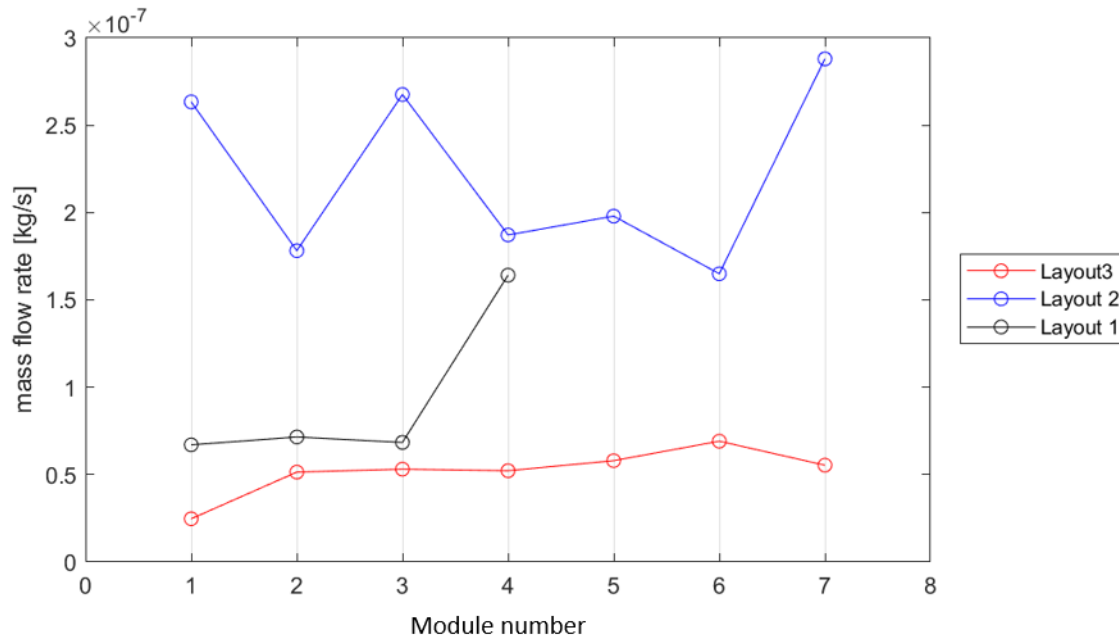

Figure 5 Mass flow rate vs Module Number for the three investigated layouts

A control volume with length of 2 mm from inlet to outlet was chosen for a qualitative modelling of the filter to examine pressure drops. 7816.88 Pa for layout in Figure 4a, 6533.65 Pa for layout in Figure 4b and 5937.01 Pa for layout in Figure 4c were the pressure drops resulting from an incoming flow rate of 20 µl/min imposed at the inlet.

The presence of closed walls in the starting geometry reasonably led to a higher pressure drops. Based on the assumption that homogeneous flow through the filter and low pressure drops could improve both the filtering and de-clogging phases, the choice was to continue to optimize fluid dynamics based on the layout of Figure 4c. Though, before further optimization, a preliminary bonding test for a 630 µm wide and 15 µm deep channel closure was performed. The width/depth ratio was proven to be excessive, leading to top cover collapse in the channel and, consequently, channel occlusion. Therefore, with a view to the subsequent fabrication process, 20 µm longitudinal walls were added between the modules along the channel, with a tilted angle of the post arrays decreased to 5.7°, as reported in Figure 6. The internal structures (as the walls here designed) are fundamental to prevent top cover collapse and channel occlusion and, in this case, also contribute to further homogenize the flow among the modules.
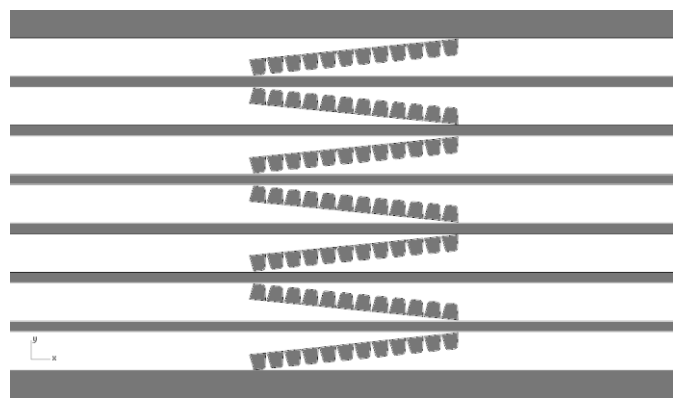
Figure 6 Fourth proposed layout with walls between tilted modules

The presence of these walls increased the computational demand due to the higher number of boundary layers and the subsequent mesh inflation along them. To avoid this problem, a single module was investigated, from here on, considering valid for the pressure drops the analogy between microfluidic device and its equivalent electric circuit [25]. In this case, the control volume, containing a single filtering module, was 75 μm wide, 15 μm high and 2 mm long (W x H x L). Results from this configuration showed a good compromise between pressure drops (57933.7 Pa along the channel) and the mass flow rate through the module, that in this case is 4.9×10^{-7} kg/s. Velocity profiles were affected by the presence of walls, more specifically by the decreasing of the cross section. While fluid flow was maintained homogeneous along all the modules, avoiding zones with lower velocities, the maximum value of velocity is much higher than the previous layouts.

The following reasonable step of this numerical study was the adjustment of some geometric parameters that could facilitate the decreasing of the pressure maintaining the same tilted array of posts and aspect ratio of the whole channel. For this aim, the number of modules were decreased to 5 and the tilted angle was set to 11.3°, as reported in Figure 7. Now, the total pore area is equal to 1950 μm^2.
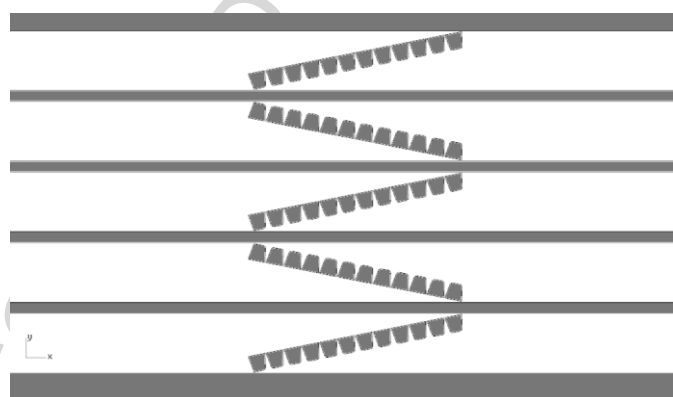

Figure 7 Fifth proposed layout with decreased number of modules with respect to fourth layout

A comparison between these two last layouts is shown in Figure 8. Following the geometric variations, the single module had a width of 110 μm. The velocity through the module of the last layout is more homogeneous than the layout with module tilting angle of 5.7°. Moreover, the peak velocity is decreased. For completeness, the velocity vector plot of the last layout is reported in the *Supplementary Material*.
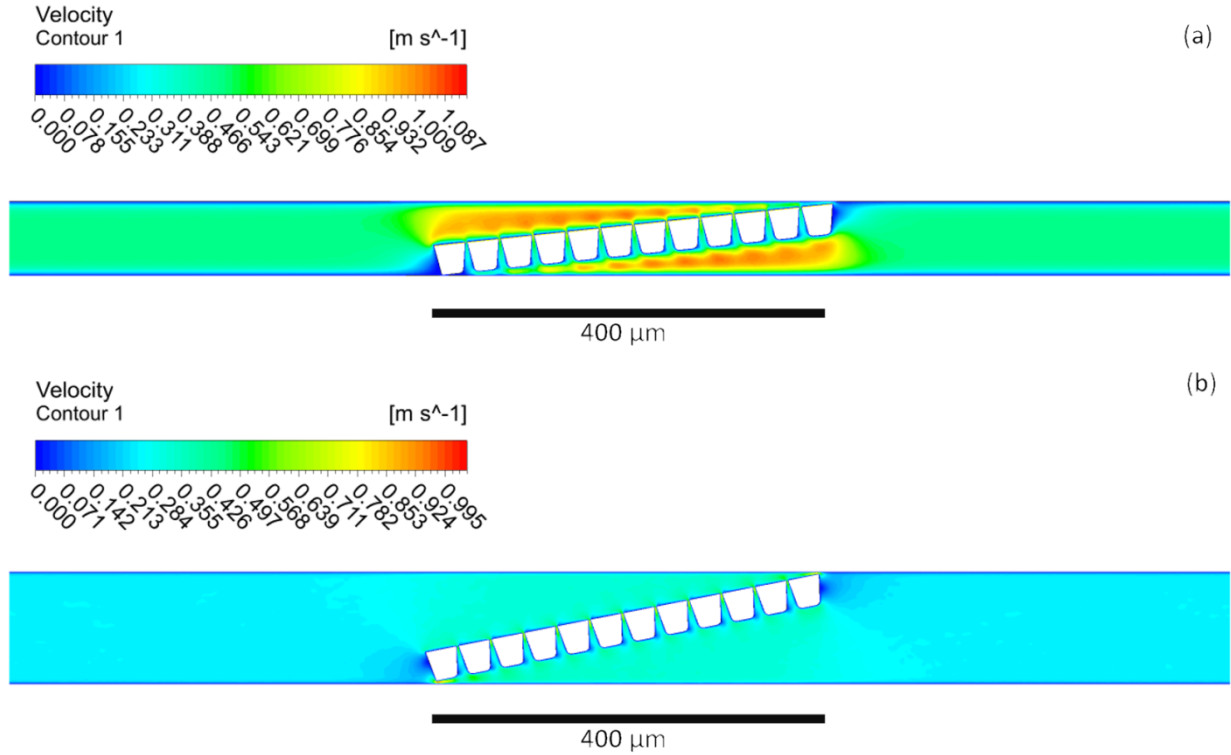
*Figure 8 Comparison of velocity contour plots of the single modules. (a) Width of the sub-channel 75 μm and angle of the filter 5.7°.
(b) Width of the sub-channel 110 μm and angle of the filter 11.3°.*

The layout reported in Figure 7 showed the best results and was chosen as candidate for prototype fabrication. For a good analogy with experimental setup, the length of the chip was now set at 1 cm, as the fabricated device. Mass flow rate through the module in this case was found to be 3.3 x 10^-7 kg/s.

The steady-state, laminar, pressure driven flow in a channel is known as Hagen-Poiseuille flow. Equation 5 links pressure drop and flow rate of a channel with a circular cross-section [36].

$$\Delta P = \frac{8\mu L Q}{\pi a^4} \qquad (5)$$

In the above equation Q is the volumetric flow rate, a is the cross-sectional radius and L is the length of the channel. Since the channel designed for this work had not a circular cross-section, the hydraulic diameter was calculated. Therefore, the equation was used as validation of the numerical model. Imposing a flow rate of 10 μl/min, the pressure drops resulting from numerical simulation was about 104701 Pa and from the Hagen-Poiseuille equation was 139795 Pa.

4.2 Fluorescence microscopy tests

Figure 9 shows three salient photograms from the images acquired during the passage of 4 μm green fluorescent particles dispersion through the filter. In Figure 9a, taken at the beginning (after 30 seconds) of dispersion withdrawal from the outlet, it is possible to appreciate that the channel is well emptied by the liquid dispersion and no bubbles formed. The latter fact is also an indication of good device thermal bonding. After 3 minutes (Figure 9b), when all the 15 μl dispersion was infused, particles appear to be completely blocked by the filter. Operating de-clogging (Figure 9c), by inverting the flow at the same flowrate, the particles were removed and no one was observed at the outlet side of the channel, further indication of efficient filtration.
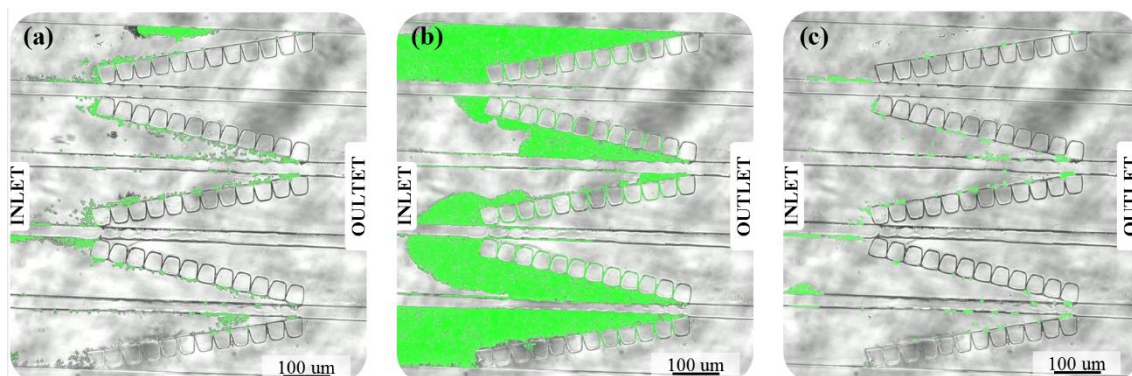
Figure 9 Photograms captured during the test. (a) First particles arrive at the filter. (b) At the end of the test the filter has trapped all the particles. (c) Particles remaining after reversal flow.

4.3   Pressure tests

Results from pressure test were encouraging. For a 10 μl/min flow rate injected inside the filtering device, a pressure drop equal to 260000 Pa was obtained. This absolute value is different from the one calculated during numerical and analytical simulations, but the order of magnitude is the same. Possible operational errors and the experimental setup deviation from numerical model could explain the pressure difference between real device and computational model.

5. Conclusions

The microfluidic filtering device object of this work was the result of an embossing process involving a single master and polymeric replicas, which guarantees two main advantages: the reproducibility of the separation devices and the employment of a polymer, surely less expensive than silicon and Pyrex and more suitable for disposable systems [20], [37], [38].

The whole device was studied to allow the de-clogging by the application of a reversal flow (from outlet to inlet) in order to improve the filtering performance with alternate cycles of filtration and cleaning and to avoid rapid irreversible clogging [39]. Primary tests performed with the optimized modules showed positive results. When fluid with a considerable number of particles was treated, filtration was proved to be highly efficient. Moreover, during the de-clogging phase, positive results were obtained allowing for an almost particle-free device, thus expanding the device life.

Further studies will involve fluidic tests with different media (e.g. plasma or plasma-like dispersion) to better understand how the media interacts with the COC device walls. Then, blood samples could be introduced to test the device in a more realistic condition. Indeed, from previous numerical investigations on the influence of fluid rheology (see *Supplementary Material*), it came that viscosity doesn't significantly affect the fluid behavior inside the device. One of the last steps could be the implementation of a passive cleaning system, that could work as a reservoir of the particles cake formed on the modules, to be tested with diluted or whole blood.

Conflicts of interest

None.

References

[1]   J. Phallen *et al.*, "Direct detection of early-stage cancers using circulating tumor DNA," *Sci. Transl. Med.*, vol. 9, no. 403, 2017.

[2]   World Health Organization, "Guide to cancer early diagnosis." 2017.

[3]   H. W. Hou, A. A. S. Bhagat, W. C. Lee, S. Huang, J. Han, and C. T. Lim, "Microfluidic devices for blood fractionation," *Micromachines*, vol. 2, no. 3, pp. 319–343, Jul. 2011.

[4]   T. Songjaroen, W. Dungchai, O. Chailapakul, C. S. Henry, and W. Laiwattanapaisal, "Blood separation on microfluidic paper-based analytical devices," *Lab Chip*, vol. 12, no. 18, p. 3392, 2012.

[5]   M. Sonker, V. Sahore, and A. T. Woolley, "Recent advances in microfluidic sample preparation and separation techniques for molecular biomarker analysis: A critical review," *Analytica Chimica Acta*, vol. 986. pp. 1–11, 2017.

[6]   P. Yager *et al.*, "Microfluidic diagnostic technologies for global public health," *Nature*, vol. 442, no. 7101. pp. 412–418, 2006.

[7]   G. C. Santini *et al.*, "miRNA purification with an optimized PDMS microdevice: Toward the direct purification of low abundant circulating biomarkers," *Biophys. Chem.*, vol. 229, pp. 142–150, Oct. 2017.

[8]   V. Vaghi *et al.*, "On-chip purification and detection of hepatitis C virus RNA from human plasma," *Biophys. Chem.*, vol. 208, pp. 54–61, Jan. 2016.

[9]   R. Riahi *et al.*, "A novel microchannel-based device to capture and analyze circulating tumor cells (CTCs) of breast cancer," *Int. J. Oncol.*, vol. 45, no. 6, pp. 1870–1878, Jun. 2014.

[10]   N. Sun, X. Li, Z. Wang, Y. Li, and R. Pei, "High-purity capture of CTCs based on micro-beads enhanced isolation by size of epithelial tumor cells (ISET) method," *Biosens. Bioelectron.*, vol. 102, pp. 157–163, Apr. 2018.

[11]   E. Sollier, H. Rostaing, P. Pouteau, Y. Fouillet, and J.-L. Achard, "Passive microfluidic devices for plasma extraction from whole human blood," *Sensors Actuators B Chem.*, vol. 141, no. 2, pp. 617–624, Sep. 2009.

[12]   A. Shamsi, A. Shamloo, N. Mohammadaliha, H. Hajghassem, J. F. Mehrabadi, and M. Bazzaz, "High throughput blood plasma separation using a passive PMMA microfluidic device," *Microsyst. Technol.*, vol. 22, no. 10, pp. 2447–2454, 2016.

[13]   J. N. Kuo and Y. H. Zhan, "Microfluidic chip for rapid and automatic extraction of plasma from whole human blood," *Microsyst. Technol.*, vol. 21, no. 1, pp. 255–261, 2015.

[14]   T. G. Kang, Y.-J. Yoon, H. Ji, P. Y. Lim, and Y. Chen, "A continuous flow micro filtration device for plasma/blood separation using submicron vertical pillar gap structures," *J. Micromechanics Microengineering*, vol. 24, no. 8, p. 087001, Aug. 2014.

[15]   I. K. Dimov, L. Basabe-Desmonts, J. L. Garcia-Cordero, B. M. Ross, A. J. Ricco, and L. P. Lee, "Stand-alone self-powered integrated microfluidic blood analysis system (SIMBAS)," *Lab Chip*, vol. 11, no. 5, pp. 845–850, 2011.

[16]   C. Potrich, L. Lunelli, M. Cocuzza, S. L. Marasso, C. F. Pirri, and C. Pederzolli, "Simple PDMS microdevice for biomedical applications," *Talanta*, vol. 193, pp. 44–50, Feb. 2019.

[17]   S. L. Marasso *et al.*, "A polymer Lab-on-a-Chip for genetic analysis using the arrayed primer extension on microarray chips," *Biomed. Microdevices*, vol. 16, no. 5, pp. 661–670, Oct. 2014.

[18]   S. Tripathi, Y. V. B. Varun Kumar, A. Prabhakar, S. S. Joshi, and A. Agrawal, "Passive blood plasma separation at the microscale: a review of design principles and microdevices," *J. Micromechanics Microengineering*, vol. 25, no. 8, p. 083001, Aug. 2015.

[19]   X. Chen, D. F. Cui, C. C. Liu, and H. Li, "Microfluidic chip for blood cell separation and collection based on crossflow filtration," *Sensors Actuators, B Chem.*, vol. 130, no. 1, pp. 216–221, 2008.

[20]   S. Thorslund, O. Klett, F. Nikolajeff, K. Markides, and J. Bergquist, "A hybrid poly(dimethylsiloxane) microsystem for on-chip whole blood filtration optimized for steroid screening," *Biomed. Microdevices*, vol. 8, no. 1, pp. 73–79, 2006.

[21]   K. H. Chung *et al.*, "Magnetically-actuated blood filter unit attachable to pre-made biochips," *Lab Chip*, vol. 12, no. 18, pp. 3272–3276, 2012.

[22]   S. Q. Wang *et al.*, "Simple filter microchip for rapid separation of plasma and viruses from whole blood," *Int. J. Nanomedicine*, vol. 7, pp. 5019–5028, 2012.

[23]   G. Maltezos, J. Lee, A. Rajagopal, K. Scholten, E. Kartalov, and A. Scherer, "Microfluidic blood filtration device," *Biomed. Microdevices*, vol. 13, no. 1, pp. 143–146, 2011.

[24]   S. Li *et al.*, "Highly efficient isolation and release of circulating tumor cells based on size-dependent

filtration and degradable ZnO nanorods substrate in a wedge-shaped microfluidic chip.," *Biomed. Microdevices*, vol. 19, no. 4, p. 93, 2017.

[25] S. Yang, A. Ündar, and J. D. Zahn, "A microfluidic device for continuous, real time blood plasma separation," *Lab Chip*, vol. 6, no. 7, pp. 871–880, 2006.

[26] Z. Geng, Y. Ju, Q. Wang, W. Wang, and Z. Li, "Multi-component continuous separation chip composed of micropillar arrays in a split-level spiral channel," *RSC Adv.*, vol. 3, no. 34, pp. 14798–14806, 2013.

[27] H. Andersson, W. Van Der Wijngaart, P. Enoksson, and G. Stemme, "Micromachined flow-through filter-chamber for chemical reactions on beads," *Sensors Actuators, B Chem.*, vol. 67, no. 1, pp. 203–208, 2000.

[28] H. M. Ji, V. Samper, Y. Chen, C. K. Heng, T. M. Lim, and L. Yobas, "Silicon-based microfilters for whole blood cell separation," *Biomed. Microdevices*, vol. 10, no. 2, pp. 251–257, 2008.

[29] J. Adler, "Ceramic diesel particulate filters," *Int. J. Appl. Ceram. Technol.*, vol. 2, no. 6, pp. 429–439, 2005.

[30] H. Bruus, "Acoustofluidics 1: Governing equations in microfluidics," *Lab Chip*, vol. 11, no. 22, pp. 3742–3751, 2011.

[31] J. Wu, Q. Yan, S. Xuan, and X. Gong, "Size-selective separation of magnetic nanospheres in a microfluidic channel," *Microfluid. Nanofluidics*, vol. 21, no. 3, pp. 1–12, 2017.

[32] S. M. McFaul, B. K. Lin, and H. Ma, "Cell separation based on size and deformability using microfluidic funnel ratchets," *Lab Chip*, vol. 12, no. 13, p. 2369, 2012.

[33] S. Aachboun and P. Ranson, "Deep anisotropic etching of silicon," *J. Vac. Sci. Technol. A*, vol. 17, no. 4, pp. 2270–2273, 1999.

[34] F. Perrucci *et al.*, "Optimization of a suspended two photon polymerized microfluidic filtration system," *Microelectron. Eng.*, vol. 195, no. February, pp. 95–100, 2018.

[35] V. Bertana *et al.*, "3D-printed microfluidics on thin poly(methyl methacrylate) substrates for genetic applications," *J. Vac. Sci. Technol. B, Nanotechnol. Microelectron. Mater. Process. Meas. Phenom.*, vol. 36, no. 1, p. 01A106, Jan. 2018.

[36] H. Bruus, "Theoretical Microfluidics (Oxford Master Series in Physics)," vol. 18, 2007.

[37] M. Quaglio *et al.*, "Evaluation of different PDMS interconnection solutions for silicon, Pyrex and COC microfluidic chips," *J. Micromechanics Microengineering*, vol. 18, no. 5, p. 055012, May 2008.

[38] S. L. Marasso, G. Canavese, and M. Cocuzza, "Cost efficient master fabrication process on copper substrates," *Microelectron. Eng.*, vol. 88, no. 8, pp. 2322–2324, Aug. 2011.

[39] J. Moorthy and D. J. Beebe, "In situ fabricated porous filters for microsystems," *Lab Chip*, vol. 3, no. 2, pp. 62–66, 2003.

Highlights: A passive two-way microfluidic device for low volume blood-plasma separation

- Starting from a particulate-trap-like filter, numerical simulations in ANSYS Fluent were performed in order to optimize the geometry for a biological sample filtration device.
- The optimized geometry was converted in a real device by employing hot embossing for polymeric replication of a single master: repeatability and cost-effectiveness are ensured.
- Filtering tests with 4 μm fluorescent beads revealed that all the particles were trapped in the filter, without causing permanent clogging of the device.